NASA Technical Memorandum 4253

Q-Circle Measurement Error

Chase P. Hearn and Edward S. Bradshaw

MAY 1991

NASA Technical Memorandum 4253

Q-Circle Measurement Error

Chase P. Hearn and Edward S. Bradshaw
Langley Research Center
Hampton, Virginia

National Aeronautics and
Space Administration
Office of Management
Scientific and Technical
Information Division

1991

Summary

This report considers the errors that accompany the application of the "Q-circle" method to resonators that are more complex than the simple resistance-inductance-capacitance (RLC) circuit, for which it was derived and is exact. The method is based on determining the ratio of the center frequency to the "intercept bandwidths" defined by the Q-circle method.

Two lumped circuits and a distributed circuit were analyzed using both symbolic and numerical methods. It was concluded that the Q-circle method can produce large errors or even fail completely, especially when measuring the loaded Q, because the impedance components of complex resonators can differ significantly from those of simple RLC resonators.

Introduction

It is an established practice to treat high-Q lumped and distributed networks near resonance as elementary three-element resistance-inductance-capacitance (RLC) circuits. The widely used "Q-circle" measurement procedure (ref. 1, p. 408) is based on this assumption. It is shown here that this assumption can lead to errors when measuring the Q-factor of more complex resonators that are heavily loaded by the external source.

In the Q-circle method, the resonator is assumed to behave as a series (or parallel) RLC circuit and the intercept frequencies are found experimentally for which the components of impedance satisfy

$$\left|\mathrm{Im}\,[Z]\right| = \mathrm{Re}\,[Z] \quad (\text{for } Q_u) \tag{1}$$

and

$$\left|\mathrm{Im}\,[Z]\right| = R_0 + \mathrm{Re}\,[Z] \quad (\text{for } Q_L) \tag{2}$$

where $\mathrm{Re}[Z]$ and $\mathrm{Im}[Z]$ are the real and imaginary parts of impedance, respectively, and Q_u and Q_L are the unloaded and loaded Q-factors, respectively. The Q-factor is then determined from

$$Q = \omega_0/\Delta\omega \tag{3}$$

where $\Delta\omega$ represents the frequency increments measured above and ω_0 denotes the resonant frequency. Equation (3) will be shown to be exact for simple series (or parallel) RLC circuits, regardless of the Q-factor, but not for more complex circuits such as in figure 1. This is shown to be due to the fact that the impedance components of the circuit vary with frequency differently from those in a pure series RLC circuit, thus causing the Q-factor determined by equation (3) to be in error.

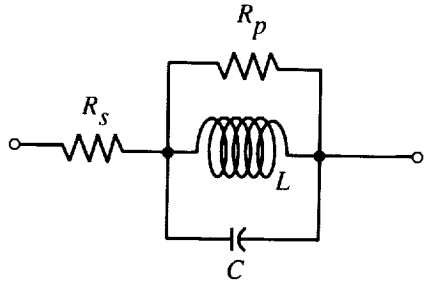

(a) Parallel resonance.

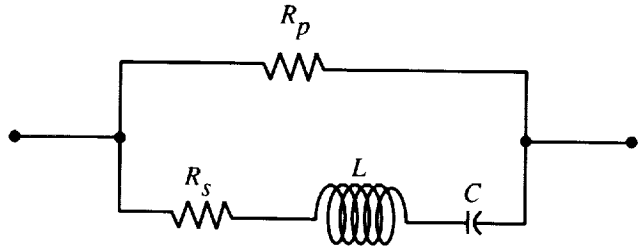

(b) Series resonance.

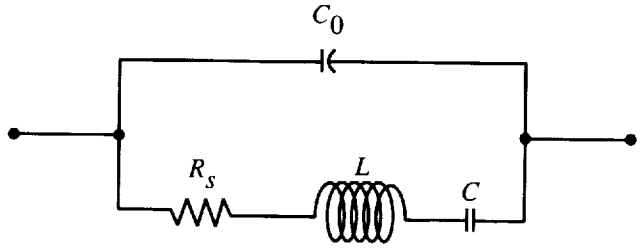

(c) Dual resonance.

Figure 1. Four-element resonant circuits.

Symbols

C	capacitance
C_{eq}	equivalent capacitance
C_0	shunt capacitance
$\mathrm{Im}\,[\,]$	imaginary part of [ ]
I_p	peak current
J	symbolic representation of algebraic expression
j	imaginary operator
K	ratio of pole-zero spacing to 3-dB semibandwidth
L	inductance
L_{eq}	equivalent inductance
ℓ	length
n	order of $\lambda/2$ resonance
$\overline{P}$	average power

Q	Q-factor
ΔQ	deviation of measured Q from actual Q
$\widehat{Q}$	Q computed from $\omega_0/\Delta\omega$
$\widetilde{Q}$	Q computed from phase slope and resonant series resistance
Q_L	loaded Q-factor
$\widehat{\widehat{Q}}_L$	Q_L computed from $\widehat{Q}_u$ and β_c
Q_u	unloaded Q-factor
Q_{u0}	series-arm unloaded Q-factor
R	resistance
Re[ ]	real part of [ ]
R_{eq}	equivalent series resistance
R_0	source resistance
R_p	shunt resistance
R_s	series resistance
t	time
V_p	peak voltage
W	peak energy
$X(\omega)$	series-arm reactance function
$Z_A(\omega)$	impedance function of circuit in figure 1(b)
$Z_B(\omega)$	impedance function of short-circuited transmission line
Z_{B0}	characteristic impedance of transmission line
$Z_c(\omega)$	impedance function of circuit in figure 1(c)
α	real part of complex propagation constant
$\alpha(\omega)$	frequency-dependent α
β	imaginary part of complex propagation constant
β_c	coupling factor
Γ	complex reflection coefficient
$\delta\omega$	pole-zero spacing
ϵ_R	relative dielectric constant
ϵ_{R0}	low-frequency value of relative dielectric constant in a dispersive medium
λ	wavelength
τ	one-way propagation time
ω	radian frequency
$\Delta\omega$	intercept bandwidth
ω_0	resonant frequency
ω_{sd}	singular frequency of denominator of $Z_c(\omega)$
ω_{sn}	singular frequency of numerator of $Z_c(\omega)$
ω_1	positive intercept frequency $\mathrm{Re}[Z(\omega)] = \mathrm{Im}[Z(\omega)]$
ω_2	negative intercept frequency $(-\mathrm{Re}[Z(\omega)] = \mathrm{Im}[Z(\omega)])$

Review: The Q-Factor of a Series RLC Circuit

As a preliminary discussion and review, equation (3) is derived for a series RLC circuit having the impedance function

$$Z(\omega) = R_s + j\left(\omega L - \frac{1}{\omega C}\right) = R_s + j\,X(\omega) \qquad (4)$$

The fundamental definition of Q is (ref. 1, p. 349)

$$Q = \frac{2\pi\ (\text{Peak energy stored})}{\text{Energy dissipated per cycle}} = \frac{\omega_0 W}{\overline{P}} \qquad (5)$$

where W is the peak energy stored and $\overline{P}$ is the average power dissipated during a period T. At a current maximum, all stored energy is in the magnetic field of L. When driven from a source resistance R_0, Q_L is given by

$$Q_L = \frac{\omega_0(LI_p^2/2)}{\left(I_p/\sqrt{2}\right)^2(R_0 + R_s)} = \frac{\omega_0 L}{R_0 + R_s} \qquad (6)$$

which is well-known. The unloaded Q (i.e., Q_u) is found from equation (6) with $R_0 = 0$. It follows that

$$\frac{Q_u}{Q_L} = \frac{R_s + R_0}{R_s} = 1 + \frac{R_0}{R_s} = 1 + \beta_c \qquad (7)$$

where the factor R_0/R_s, which is designated the coupling factor β_c in Q-circle terminology, is the ratio of power dissipated by the source resistance R_0 to that dissipated by the resonant circuit. For a series resonance, β_c is found by inverting the value on the

Smith chart where the resonant locus intersects the real axis.

In the experimental determination of Q using equation (6), R_s and ω_0 are measured directly at ω_0, but L cannot be determined by a single-frequency measurement at ω_0. The slope of the reactive part of equation (4) (i.e., $X(\omega)$) at resonance is

$$\left.\frac{dX(\omega)}{d\omega}\right|_{\omega=\omega_0} = 2L \tag{8}$$

The experimental determination of L is especially easy for the reactance function $X(\omega)$ in equation (4) because it has the interesting and useful property that the slope of all lines connecting points of equal magnitudes and opposite signs always equals the slope at resonance. That is,

$$\frac{2R}{\omega(R)-\omega(-R)} = \left.\frac{dX(\omega)}{d\omega}\right|_{\omega=\omega_0} = 2L \tag{9}$$

where $\omega(\pm R)$ are the values of the inverse function of $X(\omega)$, that is, $\omega(X)$, when $|X| = R$. Since equation (9) is true for any value of R, it must be true for $R = R_0 + R_s$; and thus Q_L (from eqs. (6), (8), and (9)) is given as

$$Q_L = \omega_0 \frac{R_0 + R_s}{\omega(R_0 + R_s) - \omega(-R_0 - R_s)} \frac{1}{R_0 + R_s} \tag{10}$$

which reduces exactly to equation (3). Thus, the Q-circle method is exact for a series (or, by duality, a parallel) RLC resonator.

Examples of Q-Circle Measurement Error

The remainder of this paper considers the consequences of applying equation (3) to lumped and distributed element resonant networks for which the $\mathrm{Re}\,[Z(\omega)]$ can vary with frequency and the reactance functions do not satisfy equation (9), on which the derivation of equation (3) and the Q-circle method are based. Three examples are presented in the following discussion.

Example 1: Lumped Element Circuit

The circuit of figure 1(a) was used in reference 1 to model the effect of coupling-circuit loss on the Q-factor measured by the voltage standing-wave ratio (VSWR) method (ref. 1, p. 413). The effect of the added loss resistance on a Q-circle measurement is carried out here for the circuit dual of figure 1(a) and is shown in figure 1(b). Although the Q of the circuit is lower with R_p than without R_p, the Q-factors computed from equation (3) will be shown to be less than the correct values, as found from equation (5).

The impedance components of the circuit of figure 1(b) are

$$\mathrm{Re}\,[Z_A(\omega)] = \frac{R_p R_s (R_p + R_s) + R_p X^2(\omega)}{(R_p + R_s)^2 + X^2(\omega)} \tag{11}$$

and

$$\mathrm{Im}[Z_A(\omega)] = \frac{R_p^2 X(\omega)}{(R_p + R_s)^2 + X^2(\omega)} \tag{12}$$

where $X(\omega)$ is the series-arm reactance function. Figure 2 is a computer-generated plot of equations (11) and (12) and illustrates how the shunt-loss element R_p modifies the behavior of a series circuit. The degradation in Q_u with $R_p = 500$ can be shown to be about 1 percent. Near resonance where $X(\omega) << R_p + R_s$, equations (11) and (12) can be closely approximated as

$$\mathrm{Re}\,[Z_A(\omega)] \approx \frac{R_p R_s}{R_p + R_s} + \frac{R_p}{(R_p + R_s)^2} X^2(\omega) \tag{13}$$

and

$$\mathrm{Im}\,[Z_A(\omega)] \approx \left(\frac{R_p}{R_p + R_s}\right)^2 X(\omega) - \frac{R_p^2}{(R_p + R_s)^4} X^3(\omega) \tag{14}$$

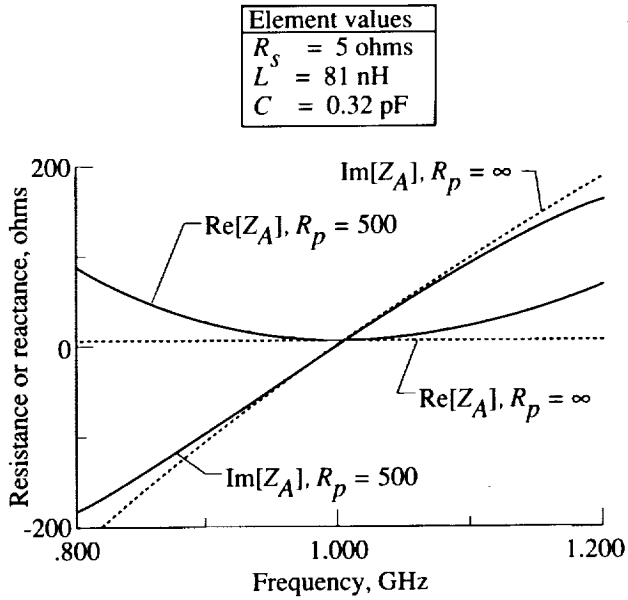

Figure 2. Components of impedance for four-element resonator.

Relative to the series arm alone, the resonant reactance slope is reduced by the factor $[R_p/(R_p+R_s)]^2$ and the series resistance is reduced by the factor $R_p/(R_p + R_s)$, resulting in a net decrease in Q_u by the factor $R_p/(R_p+R_s)$. At the frequencies satisfying equations (1) and (2), the nonlinear terms in $X(\omega)$ in equations (13) and (14) cause the behavior shown in figure 2; the experimentally determined reactance slope decreases and series resistance increases, relative to the values at ω_0. Both of these effects tend to produce a Q-factor lower than that defined by equation (5).

Figure 3 is a Smith-chart plot of $Z_A(\omega)$ that includes the Q_u and Q_L intercepts defined by equations (1) and (2). When $|X(\omega)| >> R_p$, far from resonance, the locus begins and ends inside the chart perimeter. If the frequency sweep is sufficiently wide, additional intersections with the lines $\mathrm{Im}[Z_A] = \mathrm{Re}[Z_A]$ will occur, and either a second pair of intersections—or no intersections at all—with the lines $\mathrm{Im}[Z_A] = \mathrm{Re}[Z_A] + R_0$ will occur, depending on the value of R_p. Thus, the Q-circle procedure can be in error—or even fail completely.

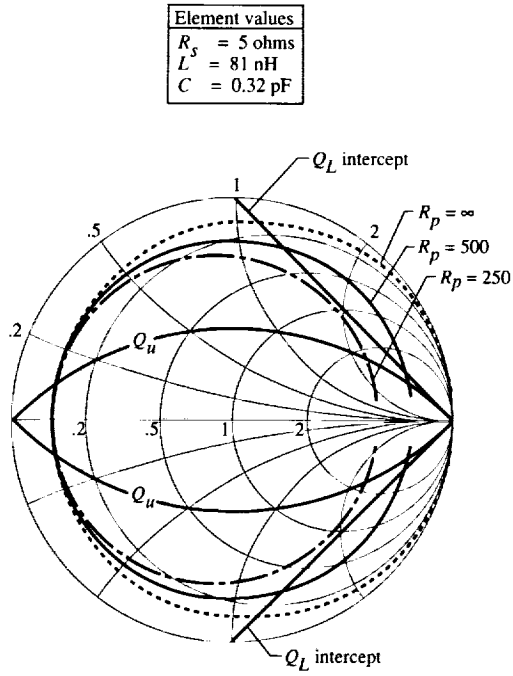

Figure 3. Smith-chart/Q-circle plot of example circuit impedance components (0.5–2 GHz).

The approach used here to evaluate the error associated with the application of equation (3) to nontrivial resonators is to find the true Q from the resonant series-equivalent circuit for comparison with Q as determined by equation (3). Regardless of the actual circuit topology, it is assumed to be exactly representable at resonance as a simple series RLC circuit, as shown in figure 4. The equivalent series resistance R_{eq} is found by evaluating equation (11) at ω_0, and the equivalent series inductance L_{eq} is found by applying equation (8) to equation (12). From equations (6) and (8), Q_L is

$$Q_L = \omega_0 \frac{\frac{d}{d\omega}\{\mathrm{Im}[Z_A(\omega)]\}_{w=w_0}}{2\ \mathrm{Re}\,[Z_A(\omega_0)]} = \frac{\omega_0 L R_p^2}{(R_p + R_s)(R_0R_p + R_0R_s + R_pR_s)} \tag{15}$$

Here, Q_u is found by letting $R_0 = 0$ in equation (15).

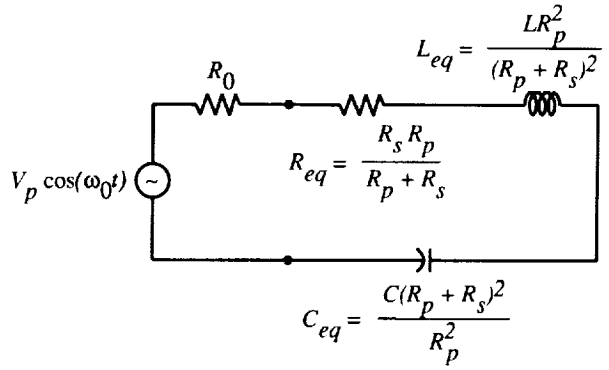

Figure 4. Series-equivalent model at resonance.

Computation of Q by using equation (3) requires an analytical determination of $\Delta\omega$. The direct application of equation (2) to equations (11) and (12) leads to a quadratic in $X(\omega)$, which is solved using a power-series representation for the radical term. The frequencies at which $X(\omega)$ has the values satisfying equation (2) are then found without further approximations. This approach avoids solving a fourth-degree polynomial. The quadratic in $X(\omega)$ with $\mathrm{Im}\,[Z_A]$ positive in equation (2) is

$$X^2(\omega) - \frac{R_p^2}{R_0 + R_p} X(\omega) + \frac{(R_p + R_s)(R_pR_s + R_0R_s + R_0R_p)}{R_0 + R_p} = 0 \qquad (X(\omega) > 0) \tag{16}$$

which has the solutions

$$X = \frac{R_p^2}{2(R_0 + R_p)} \left[1 \pm \sqrt{1 - \frac{4(R_p + R_s)(R_pR_s + R_0R_s + R_0R_p)(R_0 + R_p)}{R_p^4}} \right] \tag{17}$$

For values of R_s, R_p, and R_0 of interest, the second term under the radical is small compared to unity, and the radical is approximated by a three-term power series in the variable J, which is defined as

$$J \equiv \frac{4(R_p + R_s)(R_pR_s + R_0R_s + R_0R_p)(R_0 + R_p)}{R_p^4} \tag{18}$$

The series approximation for the radical is

$$(1 - J)^{1/2} \approx 1 - \frac{J}{2} - \frac{J^2}{8} \tag{19}$$

which is accurate to at least 2 percent when $J < 0.5$. More terms can be carried if greater accuracy is required.

The negative square root in equation (17), denoted by X_2, corresponds to the smallest positive value of $X(\omega)$ satisfying equation (2), that is, the positive root nearest resonance and the positive root of primary interest here. Using equation (19) with (17) gives

$$X_2 = \frac{(R_p + R_s)(R_pR_s + R_0R_s + R_0R_p)}{R_p^2} + \frac{(R_p + R_s)^2(R_pR_s + R_0R_s + R_0R_p)^2(R_0 + R_p)}{R_p^6} \tag{20}$$

The only approximation used in the derivation of equation (20) was the series approximation in equation (19).

Because of the symmetry characteristics of equations (11) and (12), the root of the quadratic equation corresponding to negative $\mathrm{Re}\,[Z]$ in equation (2) (i.e., X_1) is the negative of equation (20). That is, $X_1 = -X_2$. The bandwidth $\Delta\omega$ is found by solving the series-arm reactance equations

$$X_2 = \omega_2 L - \frac{1}{\omega_2 C} \tag{21}$$

and

$$X_1 = -X_2 = \omega_1 L - \frac{1}{\omega_1 C} \tag{22}$$

for $\omega_2 - \omega_1 = \Delta\omega$, which leads to

$$\Delta\omega = \frac{X_2}{L} \tag{23}$$

Following the Q-circle procedure and substituting equation (23) into equation (3) gives the measured Q_L (i.e., $\widehat{Q}_L$) as

$$\widehat{Q}_L = \frac{\omega_0 L}{X_2} \tag{24}$$

It can be seen upon combining equations (20) and (24) that $\widehat{Q}_L$ differs from Q_L in equation (15). The fractional difference between these Q-factors is found from equations (15), (20), and (24) as

$$\frac{\Delta Q_L}{Q_L} \equiv \frac{\widehat{Q}_L - Q_L}{Q_L} = -\frac{(R_p + R_s)(R_pR_s + R_0R_s + R_0R_p)(R_0 + R_p)}{R_p^4 + (R_p + R_s)(R_pR_s + R_0R_s + R_0R_p)(R_0 + R_p)} \tag{25}$$

For heavy external loading (large β_c), $R_0 >> R_s$. This simplification and assuming that $R_p >> R_s$ permits equation (25) to be approximated as

$$\frac{\Delta Q_L}{Q_L} \approx -\frac{(R_0/R_p) + (R_0/R_p)^2}{1 + (R_0/R_p) + (R_0/R_p)^2} \tag{26}$$

The error in Q_u is found by setting R_0 to zero in equation (25):

$$\frac{\Delta Q_u}{Q_u} \approx -\frac{(R_s/R_p) + (R_s/R_p)^2}{1 + (R_s/R_p) + (R_s/R_p)^2} \tag{27}$$

Thus, when $R_0 >> R_s$ the fractional error in $\widehat{Q}_u$ is much less than the error in $\widehat{Q}_L$—a fact that can be used to advantage when using the Q-circle method. An alternative to using equation (24) and the Q_L intercepts is therefore to measure $\widehat{Q}_u$ and $\widehat{\beta}_c$ and compute $\widehat{\widehat{Q}}_L$ from

$$\widehat{\widehat{Q}}_L = \frac{\widehat{Q}_u}{1 + \widehat{\beta}_c} \tag{28}$$

To the extent that $\widehat{\beta}_c$ is accurately measured, the error in $\widehat{\widehat{Q}}_L$ is that associated with $\widehat{Q}_u$, given by equation (27), as compared with equation (26) for $\widehat{Q}_L$.

Substituting equation (15) into equations (26) and (27) with R_0/R_p, R_s/R_p, and $R_s/R_0 << 1$ gives the approximations

$$\frac{\Delta Q_L}{Q_L} \approx -\frac{\omega_0 L}{Q_L R_p} \tag{29}$$

and

$$\frac{\Delta Q_u}{Q_u} \approx -\frac{\omega_0 L}{Q_{u0} R_p} \tag{30}$$

in which Q_{u0} is the series-arm Q. These equations are useful for assessing the potential measurement errors associated with known element values.

Another interesting observation can be made upon computing the degradation of Q_{u0} by R_p,

$$\frac{\Delta Q_{u0}}{Q_{u0}} = \frac{Q_{u0} - Q_u}{Q_{u0}} = 1 - \frac{Q_u}{Q_{u0}} \tag{31}$$

which is found from equation (15) with $R_0 = 0$ as

$$\frac{\Delta Q_{u0}}{Q_{u0}} = \frac{R_s/R_p}{1 + (R_s/R_p)} \tag{32}$$

A comparison of equations (32) and (27) reveals that the fractional error in measuring Q_u is approximately the same as the fractional reduction of Q_{u0} by R_p. For the element values used in figures 2 and 3, $\Delta Q_0/Q_{u0}$ and $\Delta Q_u/Q_u$ are about 0.01 and $\Delta Q_L/Q_L$ is about 0.091.

It was this disparity between $\widehat{Q}_L$ and $\widehat{\widehat{Q}}_L$ that provided the initial motivation for this work. A Hewlett-Packard (HP) 8510B vector network analyzer was automated to perform the Q-circle routine and provided a level of repeatability unobtainable with manual procedures. A systematic difference between $\widehat{Q}_L$ and $\widehat{\widehat{Q}}_L$ as large as 10 percent was observed in a variety of heavily loaded microwave resonators. This disparity might have been previously overlooked, or obscured, because of the inaccuracies associated with manual measurements.

Example 2: Distributed Circuit

The input impedance of a lossy, short-circuited transmission line is

$$Z_B(\ell) = Z_{B0} \tanh(\alpha\ell + j\beta\ell) \tag{33}$$

Figure 5 plots the computed components of impedance of a short-circuited, precision-coaxial 30-cm air line, with the loss parameter (0.0065 dB/in. at 2.6 GHz) based on measurements by the HP 8510B vector network analyzer. Figure 6 plots the impedance components of a state-of-the-art, shorted duroid microstrip transmission line (Rogers RT/duroid 5870) having the same electrical length as the air line. Both plots show multiple resonances and the conditions that produced Q-circle error in the lumped element case: $\mathrm{Re}\,[Z_B(\omega)]$ is frequency dependent and $\mathrm{Im}[Z_B(\omega)]$ does not satisfy equation (9). As in the lumped element case, $\mathrm{Re}\,[Z_B(\omega)]$ increases away from resonance, which acts to make $\widehat{Q}_u < Q_u$; in contrast, $\mathrm{Im}[Z_B(\omega)]$ results in a reactance slope measured between the intercept points that exceeds the resonant value. It will be shown that the former effect

dominates $\widehat{Q}_u$ in a transmission-line resonator, that $\widehat{Q}_u < Q_u$, and that $\widehat{Q}_L$ can in some situations exceed Q_L.

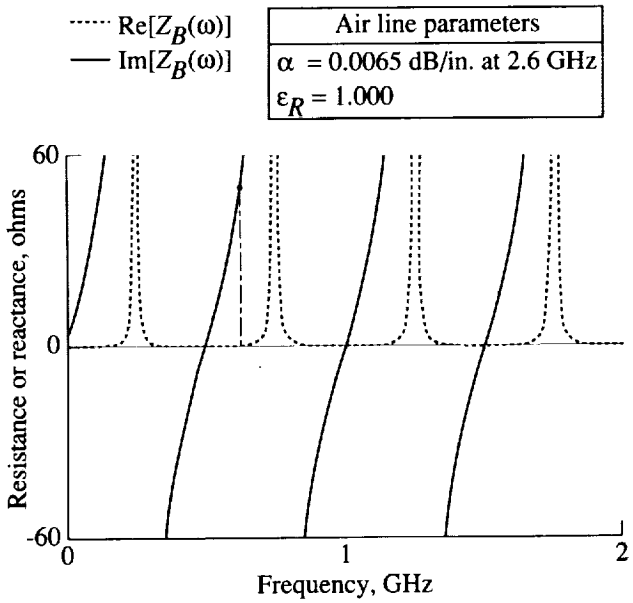

Figure 5. Components of impedance for 30 cm × 7 mm short-circuited air line.

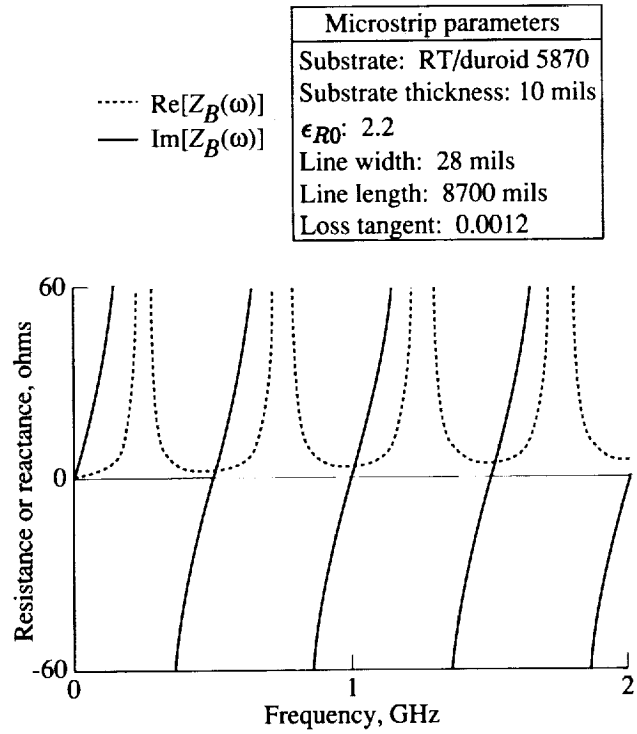

Figure 6. Components of impedance for short-circuited microstrip line.

Figures 5 also suggests that the error in measuring $\widehat{Q}_L$ might increase with the order of the resonance, which is shown to be true. An examination of figure 5 reveals that $\widehat{Q}_L$, as defined by equation (3), can be measured with the air line. The term $\mathrm{Re}\,[Z_B(\omega)]$ increases from 0.194 ohm at resonance to 0.501 ohm at the upper intercept point; the resultant error in $\widehat{Q}_L$ is less than 0.6 percent. In the microstrip line case, $\mathrm{Re}\,[Z_B(\omega)]$ increased considerably from the resonant value and is not negligible with respect to R_0. It appears that this effect will, at least initially, reduce the error in $\widehat{Q}_L$; however, an analytical expression was not derived for this case.

The analysis of the distributed-element case parallels that applied to the lumped element case: the Q-factor computed from equation (15) is compared with that computed from equation (3). Using an identity for hyperbolic functions having complex arguments and recognizing the fact that $\beta\ell = \omega\tau$ allows equation (33) to be expressed as

$$Z_B(\omega) = Z_{B0}\frac{\sinh[2\,\alpha(\omega)\,\ell] + j\sin(2\omega\tau)}{\cosh[2\,\alpha(\omega)\,\ell] + \cos(2\omega\tau)} \qquad (34)$$

for a nondispersive line, where τ is the one-way propagation time. The attenuation constant $\alpha(\omega)$ is assumed to be constant in the vicinity of each resonance, but increasing stepwise with the order of resonance. As a consequence, the derivatives of $\alpha(\omega)$ with respect to ω are zero around each resonance.

The reactance slopes of $Z_B(\omega)$ evaluated at the the nth $\lambda/2$ resonance, where $\omega\tau = n\pi$, is

$$S \equiv \frac{d}{dw}\mathrm{Im}[Z_B(\omega)]\bigg|_{\omega=n\pi/\tau} = \frac{Z_{B0}\,\tau}{\cosh^2[\alpha(\omega)\,\ell]} \qquad (35)$$

and

$$\mathrm{Re}\,[Z_B(\omega)]_{\omega=n\pi/\tau} = \frac{Z_{B0}\sinh[2\,\alpha(\omega)\,\ell]}{2\cosh^2[\alpha(\omega)\,\ell]}\bigg|_{\omega=n\pi/\tau} \qquad (36)$$

The unloaded Q defined by equation (15) is

$$Q_u = \frac{\omega\tau}{\sinh[2\,\alpha(\omega)\,\ell}\bigg|_{\omega=n\pi/\tau} = \frac{n\pi}{\sinh[2\,\alpha(\omega)\,\ell]} \qquad (37)$$

When $2\,\alpha(\omega)\,\ell << 1$, then $\sinh[2\,\alpha(\omega)\,\ell \simeq 2\,\alpha(\omega)\,\ell$ and equation (37) can be closely approximated as

$$Q_u \doteq \frac{\pi}{\alpha\lambda} = \frac{\beta}{2\alpha} \tag{38}$$

At a fixed frequency, Q_u is therefore independent of the line length and/or the order of the resonance.

The unloaded Q that would be measured using equation (3) is found by applying equation (1) to equation (34) with $\omega = (n\pi/\tau)+(\Delta\omega/2)$, which leads to

$$\sinh[2\,\alpha(\omega)\,\ell] = |\sin(\Delta\omega\,\tau)| \tag{39}$$

Equation (39) is solved for $\Delta\omega$, which is used in equation (3) to find

$$\widehat{Q}_u = \frac{\omega_0}{\Delta\omega} = \frac{\omega_0\tau}{\sin^{-1}\{\sinh[2\,\alpha(\omega)\,\ell]\}} \tag{40}$$

The ratio of $\widehat{Q}_u$ to Q_u is, from equations (37) and (40),

$$\frac{\widehat{Q}_u}{Q_u} = \frac{n\pi/Q_u}{\sin^{-1}(n\pi/Q_u)} \tag{41}$$

Since Q_u in equation (41) is essentially independent of n, higher order resonances ($n > 1$) at a fixed frequency produce greater errors in measuring Q_u according to equation (38). This can be attributed to the fact that $\Delta\omega$ becomes a larger fraction of the pole-to-pole spacing of equation (34) that decreases with increasing n. However, the error in $\widehat{Q}_u$ becomes practically significant only when $n\pi/Q_u > 0.25$, for which equation (41) is 1 percent low.

The value of $\widehat{Q}_L$ cannot always be found by the Q-circle method, as demonstrated by figure 3 with $R_P = 250$, and must be computed by using equation (15) or (28). Figure 5 represents a case for which $\widehat{Q}_L$ can be found since equation (2) can be satisfied. In this case, $\mathrm{Re}\,[Z(\omega)]$ is entirely negligible compared with R_0 over the full Q_L intercept bandwidth.

Here, Q_L is found from equations (15) and (35) with $\alpha(\omega) = 0$ and is given as

$$Q_L = \frac{\omega_0 Z_{B0}\,\tau}{2R_0} = \frac{n\pi Z_{B0}}{2R_0} \tag{42}$$

and $\widehat{Q}_L$ is found by determining the $\Delta\omega$ for which

$$R_0 = \frac{Z_{B0}\sin(2\omega\tau)}{1+\cos(2\omega\tau)} = Z_{B0}\tan(\omega\tau) \tag{43}$$

when $\omega = (n\pi/\tau) + (\Delta\omega/2)$, as indicated by the vertical dashed line in figure 5 ($n = 1$; $R_0 = 50$). This is found to be

$$\Delta\omega = \frac{2}{\tau}\tan^{-1}\left(\frac{R_0}{Z_{B0}}\right) \tag{44}$$

which is used in equation (3) to get

$$\widehat{Q}_L = \frac{n\pi}{2\tan^{-1}(R_0/Z_{B0})} \tag{45}$$

In contrast to $\widehat{Q}_u$, $\widehat{Q}_L > Q_L$ since the only error in equation (45) was due to the slope measurement, which was larger than the correct, or resonant, value. Equation (45) is applicable only if $\mathrm{Re}\,[Z_B(\omega)] << R_0$ at the intercept points. Subject to this restriction, equation (45) is independent of the absolute value of Q_L, which can be made arbitrarily large by increasing n in equation (42). For example, with $n = 10$ and $R_0/Z_{B0} = 0.5$, $Q_L = 31$ and $\widehat{Q}_L$ is 8 percent high.

Example 3: Dual Resonance

The circuit of figure 1(c) has two resonances, with the desired resonance an impedance zero and the adjacent resonance an impedance pole. The presence of the adjacent complementary resonance can significantly affect the value of $\widehat{Q}_u$, to the point that a measurement by equation (3) is not possible. The additional reactive element results in a fourth-order impedance function, as with the circuit of figure 1(a); however, the equation that arises from equating the real and imaginary parts of $Z_c(\omega)$ in equation (1) is not easily reducable as was the case with $Z_B(\omega)$, corresponding to figure 1(b). Therefore, this case is analyzed by essentially numerical methods. A computer model is evaluated to determine the Q-factors computed by equation (3) for comparison with those computed from equation (15).

The circuit of figure 1(c) has the impedance function

$$Z_c(\omega) = \frac{R_s + j[\omega L - (1/\omega C)]}{1 + (C_0/C) - \omega^2 LC_0 + j\omega R_s C_0} \tag{46}$$

For mathematical simplification, define the singular frequencies of equation (46) as

$$\omega_{sn}^2 \equiv \frac{1}{LC} \tag{47}$$

where the numerator is purely real, and

$$\omega_{sd}^2 \equiv \frac{C_0 + C}{LCC_0} \tag{48}$$

where the demoninator is purely imaginary. These are not the exact series or parallel resonant

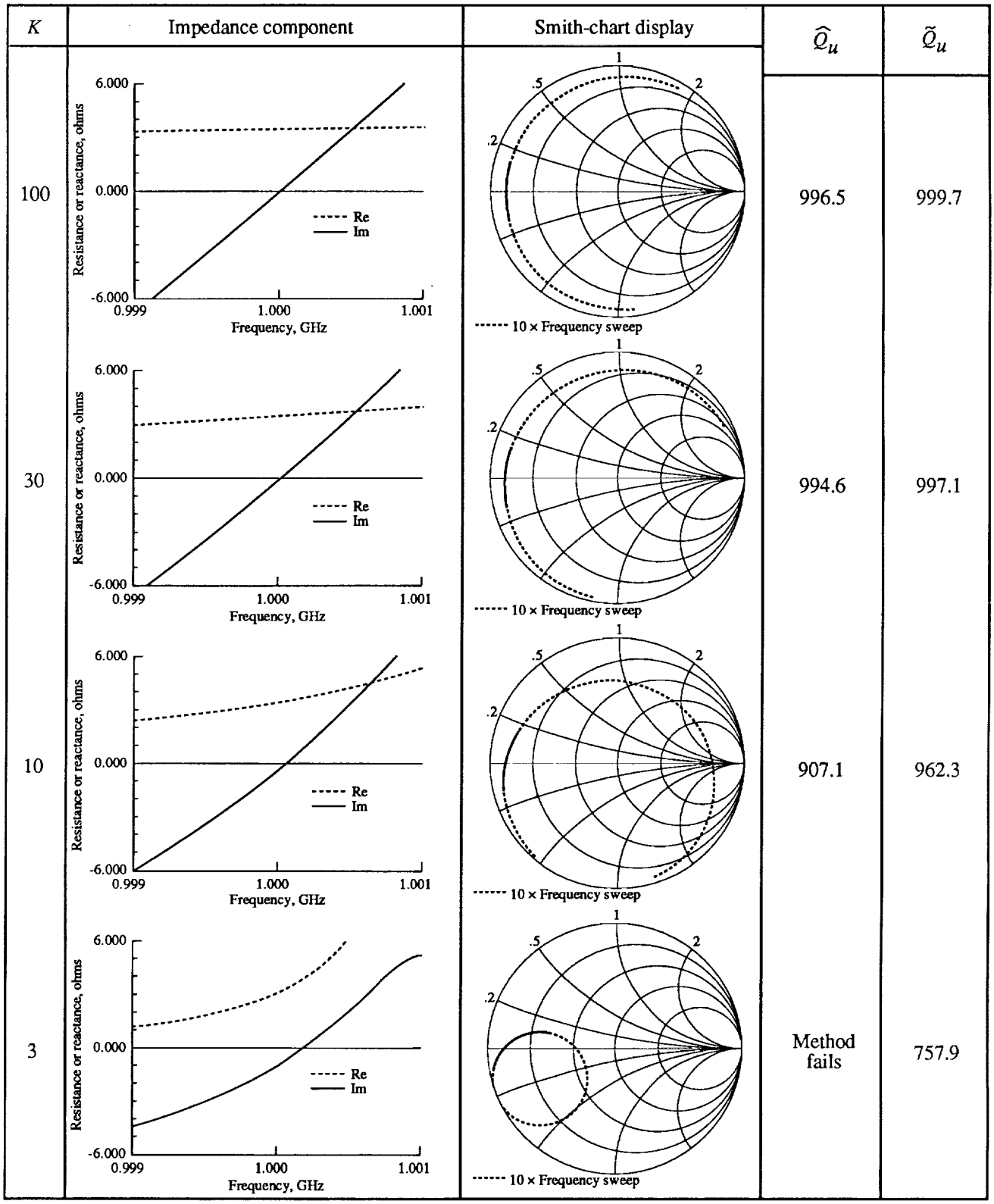

Figure 7. Theoretical Z- and Γ-plane resonance characteristics for circuit in figure 1(c) with complementary resonance K 3-dB semibandwidths above ω_{sn}.

frequencies—at which $Z_c(\omega)$ is purely real—except when R_s is zero; however, it has been observed that the values computed by equations (46) and (47) are, for practical purposes, the same as those exhibited by the model over a wide range of parameters when $Q_{u0} > 100$. In other words, the deviations of ω_{sn} and ω_{sd} from the actual series and parallel resonant frequencies are small compared with the semibandwidth of the series arm (ω_{sn}/Q_{u0}) alone.

To facilitate model evaluation, it is desirable to derive a relationship between C_0 and the spacing between the series and parallel resonances, $\delta\omega$. It follows from

$$\delta\omega \equiv \omega_{sd} - \omega_{sn} \tag{49}$$

and some manipulation of equations (47) and (48) that

$$\delta\omega = \omega_{sn}\left[\sqrt{1 + (1/LC_0\omega_{sn}^2)} - 1\right] \tag{50}$$

which is normalized to the series-arm 3-dB semibandwidth, $\Delta\omega/2Q_{u0}$, and the result is defined as K:

$$K \equiv \frac{\delta\omega}{\Delta\omega/2} = 2Q_{u0}\left[\sqrt{1 + (C/C_0)} - 1\right] \tag{51}$$

Solving equation (51) for C/C_0 gives

$$\frac{C}{C_0} = \left(\frac{K}{2Q_{u0}+1}\right)^2 - 1 \approx \frac{K}{Q_{u0}} \quad (Q_{u0} \le 0.1) \tag{52}$$

The L, C, and R_s in figure 1(c) were selected to give a series-arm Q_u (i.e., Q_{u0}) of 1000, and C_0 varied in increments computed by equation (52) to locate the pole K semibandwidths away from the zero. The behavior with respect to K of the Z-plane components and the corresponding Γ-plane locus is cataloged in figure 7, and all Z-plane data are plotted together in figure 8 for $K = 100$, 30, 10, and 3.

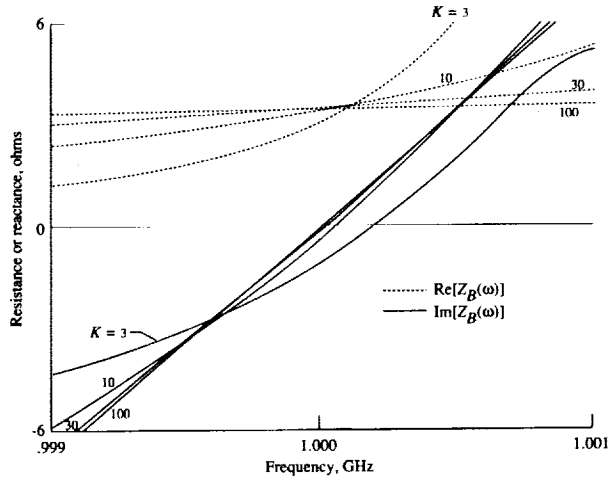

Figure 8. Components of impedance with adjacent singularity.

In all cases, $\mathrm{Re}\,[Z(\omega)]$ is not symmetrical around the frequency at which $\mathrm{Im}\,[Z(\omega)] = 0$. With $K < 10$, it is clear from figure 8 that relative to $K = 100$, the resonant frequency is shifting upward (producing a larger R_{eq}) and the reactance slope is decreasing (corresponding to a smaller L_{eq}) as defined by equation (8); Q_u is unquestionably lowered by the adjacent pole. For $K = 3$, resonance detuning is about 25 percent of the 3-dB semibandwidth, L_{eq} is increased by 15 percent, and the resonant reactance slope is decreased by 13 percent. Furthermore, this extreme case could not be measured by equation (3) since there is no intersection with $\mathrm{Re}\,[Z_c(\omega)]$ when $\mathrm{Im}\,[Z_c(\omega)]$ is positive.

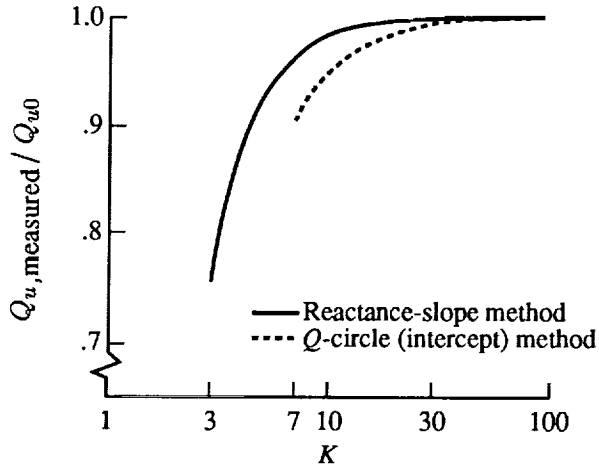

Figure 9. Unloaded Q determined using intercept bandwidth and phase-slope methods with adjacent secondary resonance K 3-dB semibandwidths away.

The Q-factors defined by equations (3) and (15) were computed from linearly interpolated, computer-generated impedance data for the pole-zero separations listed above. The reactance slope was approximated over the center 10 percent of the 3-dB bandwidth, and the Q that was computed from equation (15) was taken as the correct value. The $K = 100$ case is essentially the same as $K = \infty$ and indicates that the computational accuracy is better than 1×10^{-3}. These results are plotted in figure 9, where it can be seen that the difference in Q_u from equations (3) and (15) is about 3 percent when $K = 10$ and 0.3 percent when $K = 30$; thus it is advisable to ensure that K is 30 or more before using equation (3).

Discussion of Results

The Q-circle method for experimentally determining Q from measured impedance data was shown to be in error for three resonant circuit configurations

more complex than a simple series or parallel RLC circuit. Two of these circuits were chosen for their ease of analysis, and the third was evaluated numerically with a computer model. Q-circle measurement error was shown to be a consequence of the components of impedance not satisfying the conditions necessary for $\omega_0/\Delta\omega$ to exactly equal the Q-factor. Lumped and distributed circuit examples were cited; and $\Delta Q/Q$, the fractional difference between $\omega_0/\Delta\omega$ and the true Q-factor, was determined.

From a practical standpoint, errors in $\widehat{Q}_u$ were shown to be insignificant unless (1) the lumped circuit Q-factor was low ($Q_u < 100$), (2) the characteristic impedance of a transmission-line resonator was less than the source impedance and/or the resonance of very high order ($n >> 1$), or (3) a complementary resonance was located within thirty 3-dB semibandwidths of the desired resonance. However, it was demonstrated that the Q-circle method can produce very large errors in Q, particularly in Q_L, and even fail completely in some situations. The factor $\Delta Q/Q$ was shown to vary inversely with the true Q-factor and, therefore, to be proportional to the intercept bandwidth. That is, the lower the Q-factor the greater the difference between $\omega_0/\Delta\omega$ and the true Q-factor.

Numerical evaluation was applied to a four-element circuit having a closely adjacent complementary impedance singularity near the desired resonance, as in a piezoelectric-crystal equivalent circuit. The radical distortion of the impedance characteristic relative to a simple RLC produced a 3-percent error in $\widehat{Q}_u$ for a singularity ten 3-dB semibandwidths away from the desired resonance.

Overall, if a disparity was observed between $\widehat{Q}_u$ as determined from equation (3) and that as computed from equation (15), or if a disparity was observed between $\widehat{Q}_L$ and the value computed from equation (28) with $\widehat{Q}_u$ and β_c, it was concluded that the latter results from both cases should be considered the more accurate.

Concluding Remarks

This report has considered the errors that accompany the application of the "Q-circle" method to resonators that are more complex than the simple resistance-inductance-capacitance (RLC) circuit, for which it was derived and is exact. The method is based on determining the ratio of the center frequency to the "intercept bandwidths" derived by the Q-circle method.

Two lumped circuits and a distributed circuit were analyzed using both symbolic and numerical methods. It was concluded that the Q-circle method can produce large errors or even fail completely, especially when measuring the loaded Q, because the impedance components of complex resonators can differ significantly from those of simple RLC resonators.

NASA Langley Research Center
Hampton, VA 23665-5225
February 5, 1991

Reference

1. Ginzton, Edward L.: *Microwave Measurements.* McGraw-Hill Book Co., Inc., 1957, pp. 349, 408, and 413.

NASA
National Aeronautics and Space Administration

Report Documentation Page

1. Report No.	2. Government Accession No.	3. Recipient's Catalog No.
NASA TM-4253		

4. Title and Subtitle	5. Report Date
Q-Circle Measurement Error	May 1991
	6. Performing Organization Code

7. Author(s)	8. Performing Organization Report No.
Chase P. Hearn and Edward S. Bradshaw	L-16821

9. Performing Organization Name and Address	10. Work Unit No.
NASA Langley Research Center Hampton, VA 23665-5225	506-44-21-03
	11. Contract or Grant No.

12. Sponsoring Agency Name and Address	13. Type of Report and Period Covered
National Aeronautics and Space Administration Washington, DC 20546-0001	Technical Memorandum
	14. Sponsoring Agency Code

15. Supplementary Notes

16. Abstract

High-Q lumped and distributed networks near resonance are generally modeled as elementary three-element resistance-inductance-capacitance (RLC) circuits. The widely used "Q-circle" measurement procedure is based on this assumption. It is shown here that this assumption can lead to errors when measuring the Q-factor of more complex resonators, particularly when heavily loaded by the external source. In the Q-circle method, the resonator is assumed to behave as a series (or parallel) RLC circuit, and the intercept frequencies are found experimentally at which the imaginary part of the impedance equals the real part of the impedance for the unloaded Q and the imaginary part of the impedance equals the real part of the impedance plus the source resistance for the loaded Q. The Q-factor is then determined as the ratio of the resonant frequency to the intercept bandwidth. This relationship is exact for simple series or parallel RLC circuits, regardless of the Q-factor, but not for more complex circuits. This is shown to be due to the fact that the impedance components of these circuits vary with frequency differently from those in a pure series RLC circuit, thus causing the Q-factor as determined above to be in error.

17. Key Words (Suggested by Author(s))	18. Distribution Statement
Q-factor measurement errors	Unclassified—Unlimited Subject Category 33

19. Security Classif. (of this report)	20. Security Classif. (of this page)	21. No. of Pages	22. Price
Unclassified	Unclassified	12	A03

For sale by the National Technical Information Service, Springfield, Virginia 22161-2171